Combining Deep-learned and Hand-crafted Features for Segmentation, Classification and Counting of Colon Nuclei in H&E Stained Histology Images

Pranay Dumbhare, Yash Dubey, Vedant Phuse, Ankush Jamthikar, Himanshu Padole, and Deep Gupta[0000−0002−7408−656X]

Department of Electronics and Communication Engineering
Visvesvaraya National Institute of Technology, Nagpur-440010, India
chaitanydumbhare21@gmail.com, deepgupta@ece.vnit.ac.in

Abstract. Colon nuclei detection within Haematoxylin & Eosin (H&E) stained histology images is important to mitigate abnormalities or diseases like colon cancer in its early stages. Therefore, the objective of the proposed work is to perform the colon nuclei segmentation, classification, and counting of the nuclei or cellular composition. This paper presents a hybrid deep learning model that combines deep-learned features obtained from the ResNet50-based model with the handcrafted features. The proposed work uses the horizontal and vertical net (HoVer-Net) as baseline model presented by the CoNIC2022 challenge team and modified it to incorporate handcrafted features obtained using two feature descriptors such as local binary patterns and the histogram of oriented gradients. The proposed model is trained and validated using the CoNIC2022 dataset. The proposed model shows a significant improvement over the baseline HoVer-Net model in segmentation and classification as well as nuclei counting tasks. The proposed work demonstrates the usefulness of combining deep features with the handcrafted features in the colon nuclei identification task.

Keywords: Colon nuclei segmentation, HoVer-Net, Deep learning, Local binary pattern, Histogram of oriented gradients

1 Introduction

The manual assessment of Haematoxylin and Eosin (H&E) stained histology slides suffers from intra- or inter-observer variability [1]. To overcome these challenges in the visual assessment of tissues, there is a growing interest in digital pathology [2], which uses a class of histology images that are used to generate the whole slide images (WSI). Each WSI contains several nuclei of cells of different types, which can be analyzed to predict the clinical outcomes and grade the type of diseases, such as cancer [3]. Efficient segmentation and detection of nuclei cell types can provide important diagnostic information about the tissues

that contribute to disease growth. This was the idea behind the CoNIC2022 challenge [4], which specifically required segmenting and classifying the colon nuclei as well as finding the cellular composition by counting the different types of nuclei present in the cells. Nuclei segmentation is a challenging task because of the heterogeneous nuclear shapes, sizes, structures, as well as overlapping nuclei clusters.

Similar to nuclei segmentation, nuclei classification is also an important task that can classify different types of cells. Currently, the colon cancer diagnosis is based on the human examination of relevant histopathological images by trained pathologists. This process is time-consuming and associated with intra-or inter-observer variability [5].

Artificial intelligence (AI) is gaining popularity in almost every domain and has greatly contributed to the field of healthcare including computational pathology. In recent years, several automated AI-based systems have been proposed for nuclei detection tasks. Hamad et al. [6] proposed a convolution neural network (CNN)-based system for colon nuclei classification using H&E stained histology images. Another study used the spatially constrained CNN that predicts the probability of any pixel being the centre of the nucleus [7]. Hofener et al. [8] proposed a deep learning-based approach to predict the proximity map of histological image pixels with the centre of nuclei. Most recently, Graham et al. [9] proposed a deep learning-based model called horizontal and vertical net (HoVer-Net) to simultaneously segment and classify nuclear occurrences in histology images. The HoVer-Net model is based on the prediction of horizontal and vertical distances between nuclear pixels and their centre of mass, which are further used to separate the grouped nuclei. The nuclear type is then determined for each segmented instance using a specialized up-sampling branch.

Motivated by this automatic segmentation, classification, and nuclei composition characteristics, we propose a modified architecture of the baseline HoVer-Net model by fusing the deep-learned features and handcrafted features. Although the deep learning-based model is self-sufficient to extract features from images (so-called deep features), recent studies have shown an improvement in the segmentation and classification tasks by using the predefined texture-based handcrafted features [10]. Therefore, we hypothesized that combining handcrafted features with deep features may result in an improvement in nuclei segmentation and classification tasks.

2 Methodology

2.1 Data Pre-processing and Augmentation

In the proposed work, the dataset provided by CoNIC2022 challenge is considered [4]. The CoNIC dataset is comprised of 4981 patches of size $256\times256\times3$ RGB extracted from the Lizard dataset [11], which contains the image sections from the colon tissues. Each RGB image patch is associated with an instance segmentation map and a classification map, as shown in Fig. 1. The instance segmen-

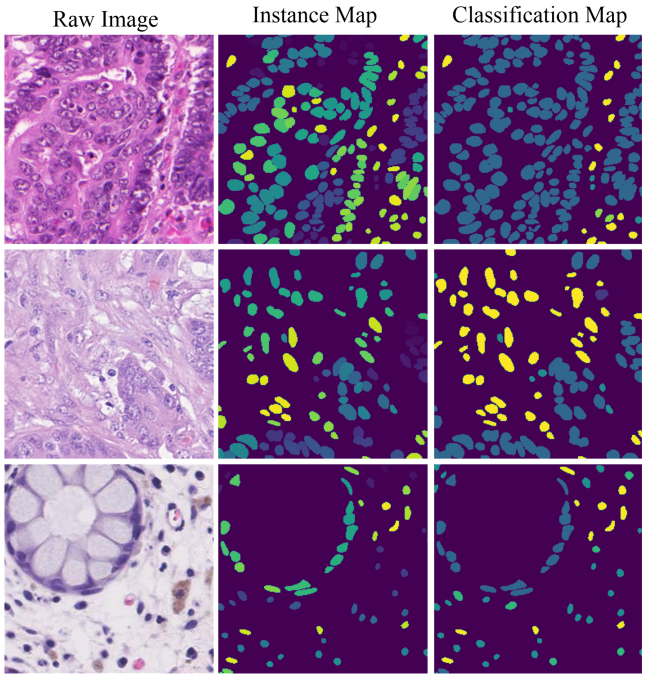

Fig. 1. Sample input images with the corresponding segmentation and classification maps

tation map holds values ranging between 0 (background) and N (number of nuclei) that label each nucleus. Similarly, the classification map holds values ranging between 0 (background) and C (number of classes) that provides the class for each pixel within the patch. In total there are six nuclei classes such as neutrophil, epithelial, lymphocyte, plasma, eosinophil, and connective tissue. These six nuclei classes and the background are used in the classification task. The size of the instance segmentation/classification map is $4981 \times 256 \times 256 \times 2$, with the first channel being the instance segmentation map and the second channel being the classification map. Both RGB images and the segmentation/classification maps are provided in the form of a .npy files and augmentation is done further using Gaussian blur [12] and median blur [13] operations. In a Gaussian blur, an input image is convolved with a Gaussian low-pass filter and generates the generic blurry image. In a median blur, the central element of the filter area in the image is replaced by the median value of surrounding pixels. Besides these operations, augmentation is also performed by perturbing the hue, saturation, contrast, and brightness of the input images. All these operations are performed on the training dataset so that the model has enough variety of data for training, and the features can be identified by the model with relatively higher ease.

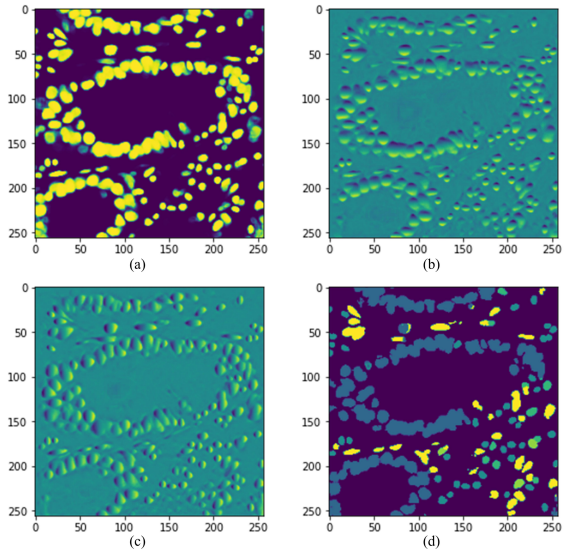

Fig. 2. The sample outputs from the three decoder branches of baseline HoVer-Net model. (a) Nuclei pixel map from the NP branch, (b and c) horizontal and vertical distance maps from the HoVer branch, and (d) nuclei classification map from the NC branch

2.2 HoVer-Net Baseline Model

The proposed study modifies the architecture of the baseline HoVer-Net model [9] for colon nuclei segmentation, classification, and counting tasks. The baseline HoVer-Net model was primarily designed for colon nuclei segmentation and showed better performance compared to the state-of-the-art studies [9]. To perform simultaneous segmentation and classification, HoVer-Net model takes advantage of the information encoded within both the vertical and horizontal distances of nuclear pixels to their centre of mass which are useful to separate the overlapping nuclei instances in the segmentation task. Then for each segmented instance, HoVer-Net model predicts the type of nucleus using a set of decoder branches. The better performance for the HoVer-Net model is attributed to the presence of three decoders such as such nuclear pixel (NP) branch, the HoVer branch (HV), and the nuclear classification branch (NC). The NP branch detects nuclei (Fig. 2 (a)), the HV branch predicts the horizontal and vertical distances of nuclear pixels to the centre of mass (Fig. 2 (b and c)), and the NC branch classifies the different types of nuclei (Fig. 2 (d)). The sample outputs of these three decoder branches are shown in Fig. 2.

2.3 Proposed Model

This section deals with the proposed model which fuses two unique types of texture-based features with deep-learned image representations. The modified

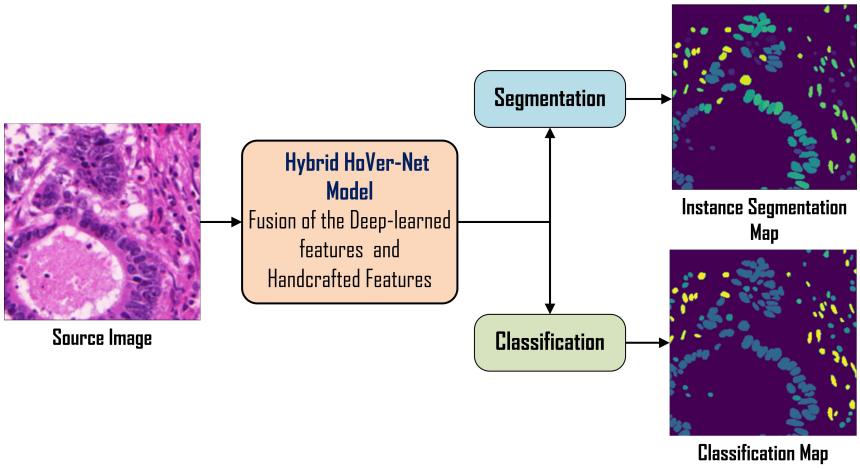

Fig. 3. The block diagram of the proposed hybrid deep learning model that demonstrates the working of the model on each individual image on the dataset

architecture is named as hybrid HoVer-Net model. The extracted features from the conventional feature descriptors, when used on their own are known to reflect on very limited aspects, as mentioned by Nguyen et al. [14], and hence are not able to do much. On another end, convolutional neural network-based models also provide good results with approx. 90% accuracy. However, as per results reported in Dalal et al. [15], Aziz et al. [16] and Song et al. [17], we observed that the accuracy can be increased to 94-99% by fusing the handcrafted features with machine learning models.

The proposed model works as described in the block diagram shown in Fig. 3. It takes the H&E stained cell patch as an image input and then performs segmentation as well as classification to provide the corresponding maps, i.e. the Instance Segmentation Map and Classification Map. Fig. 4 shows the architecture of the proposed model, which has two parts (a) encoder and (b) decoder. The encoder hosts the pre-activated residual network with 50 layers (ResNet50) and the decoder contains three different parallel layered architectures for accurate segmentation and classification of the nuclei pixels. ResNet50 is popular architecture and has shown excellent performance in several computer vision applications. Therefore, it is adopted in the encoder for feature extraction. The ResNet50-based encoder provides the image representations of size $2048 \times 32 \times 32$. These image representations extracted by the encoder are also called deep features.

In the proposed model, a branch parallel to the ResNet50-based encoder is also added to obtain the handcrafted features from two popular predefined feature descriptors viz. local binary patterns (LBP) [18] and the histogram of oriented gradients (HoG) [15]. The choice of these feature descriptors in colon nuclei identification is motivated by their efficacy in different applications e.g.

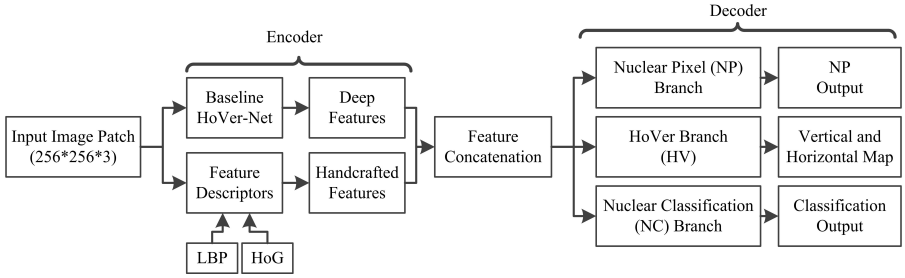

Fig. 4. The global view of the proposed hybrid deep learning model

Song et al. [17] for lung lesion detection and Aziz et al. [16] for mitotic nuclei. Multiple experimental results obtained by Li Song et al [17] for lung lesion detection, and by Aziz Et Al [16] for mitotic nuclei, corroborate the fusion of HoG and LBP features with features extracted by machine/deep learning techniques.

In the decoder, the nuclear pixel (NP) branch predicts whether a pixel belongs to the nucleus or background. The HoVer branch predicts the horizontal and vertical distances of nuclear pixels to their centres of mass. Finally, the nuclear classification (NC) branch predicts the type of nucleus for each pixel and thus facilitates cellular composition by counting the nuclei. The proposed model is trained for 10 epochs over 3963 images and was then validated on the remaining 1018 images as provided in the CoNIC2022 challenge dataset.

2.4 Handcrafted Feature Descriptors

As mentioned above, two popular feature descriptors, two popular feature descriptors i.e LBP and HoG are used in the proposed hybrid HoVer-Net model to generate handcrafted feature representations to reflect the sharp edges as in H&E staining technique is utilized in histopathological images to enhance the contrast in samples and this sharp contrast gives rise to the sharp edges. LBP is a simple yet very efficient texture descriptor, which considers a binary pattern from the surrounding pixels to decide the centre pixel intensity [18]. In the proposed hybrid HoVer-Net model, LBP feature map of dimensions 1×1024 is obtained. To match the dimension of the deep features (i.e. $2048\times32\times32$), LBP feature map of size 1×1024 is converted into the size $1\times32\times32$, giving a single feature map of dimension 32×32. on another end, HoG focuses on the structures or the shapes of objects in the input image. HoG can provide the edge directions as well. This is done by extracting the gradient and orientation (magnitude and direction) of the edges. The steps involved in HoG feature extraction are:

1. Pre-processing and reshaping the input image to size 64×128.
2. Calculating gradients (direction x and y) for a particular pixel.
3. Calculating the magnitude and orientation of gradients.
4. Creating histogram using gradients and orientation.
5. Normalizing the gradients.

6. Calculating the features for the complete image.

In the proposed model, HoG descriptor provides 33 feature maps of dimensions 32×32. These 33 feature maps from HoG and one feature map from LBP descriptor are then concatenated with deep features (2048) making the final 2082 feature maps each of dimension 32×32. These feature maps are then fed to the three decoder architectures of the proposed hybrid HoVer-Net model. The number of channels have been modified from 2048 to 2082 to improve the performance of segmentation, classification and counting of nuclei in histology images.

The other candidates such as GLCM [19], DWT [20], BRIEF [21], and ORB [22] were also considered for handcrafted feature extraction. The features were extracted using the above-listed feature extractors as well. However, the extracted features like ORB and BRIEF were not giving us the promising results as expected, thus not considered in the proposed study.

3 Experimental Details

3.1 Implementation and Parameter Settings

In the proposed model the HoG feature descriptor provides 33 feature maps of dimensions 32×32. For LBP the radius was set to 8 and the number of data points were set to 1022. To concatenate the handcrafted features with the deep features the dimensions of the output channels were changed from 2048 to 2082. The learning rate for the ADAM optimizer used here was 0.0001, and the batch size used for the training and validation of the model was 6.

3.2 Quantitative Performance Metrics

1. PQ and mPQ^{+}: Panoptic Quality (PQ) is used to assess the performance of nuclear instance segmentation. It is defined as:

$$PQ = DQ \times SQ \tag{1}$$

where DQ and SQ refer to detection quality and segmentation quality, respectively, which are given by,

$$DQ = \frac{|TP|}{|TP| + \frac{1}{2}|FP| + \frac{1}{2}|FN|} \tag{2}$$

where TP denotes true positive, FP denotes false positive, and FN denotes false negative.

$$SQ = \frac{\sum_{(x,y)\in TP} IoU(x,y)}{|TP|} \tag{3}$$

where x denotes a ground truth segment, y denotes a prediction segment and IoU denotes intersection over union that is formulated as,

$$IoU = \frac{TP}{TP + FP + FN} \tag{4}$$

For $IoU(x, y) > 0.5$, each (x, y) pair is uniquely matched over the entire set of prediction and ground truth segments [23]. This unique matching generates matched pairs (TP), unmatched ground truth segments (FN), and unmatched predicted segments (FP) for a particular type t. Hence we define multi-class PQ (mPQ^+), which takes the average of PQ over all classes T:

$$mPQ^+ = \frac{1}{T}\sum_t PQ_t \tag{5}$$

2. R^2: R^2 is a goodness-of-fit metric that measures the relationship strength between model's prediction ($\hat{y}_i$) and ground truth (y_i) on the scale of 0 to 1. The closer the value of R^2 to 1, better is the model fitted. It is also called the coefficient of determination.

$$R^2 = 1 - \frac{\sum (y_i - \hat{y}_i)^2}{\sum (y_i - \bar{y})^2} \tag{6}$$

where $\bar{y}$ is the mean of predicted counts.

3. *Mean Squared Error* (MSE) : It is the average of the squares of the the differences between the actual values and the predicted values by a model.

$$MSE = \frac{1}{D}\sum_{i=1}^{D}(x_i - y_i)^2 \tag{7}$$

where D is the number of terms, and x_i and y_i are the actual values and the predicted values respectively.

4. *Dice Score*: Dice Score is a measure of accuracy. It is used to evaluate the performance of segmentation models. It is a measure of how similar the objects are to each other.[24].

$$Dice = \frac{2 \times TP}{(TP + FP) + (TP + FN)} \tag{8}$$

Dice score lies between 0.00 to 1.00, with higher dice score indicating the better model prediction. Dice score greater than 0.8 is generally considered to be a good score.

4 Results and Discussion

The proposed hybrid deep learning model performs segmentation, classification, and the counting of nuclei from histology images by fusing the deep features with handcrafted features. Table 1 compares the proposed model with the original baseline HoVer-Net model for 10 epochs and shows a consistent improvement by the proposed model in terms of PQ, mPQ^+, and R^2 metrics. On training for 10 epochs, the proposed model demonstrates an improvement of 1.71% (0.606

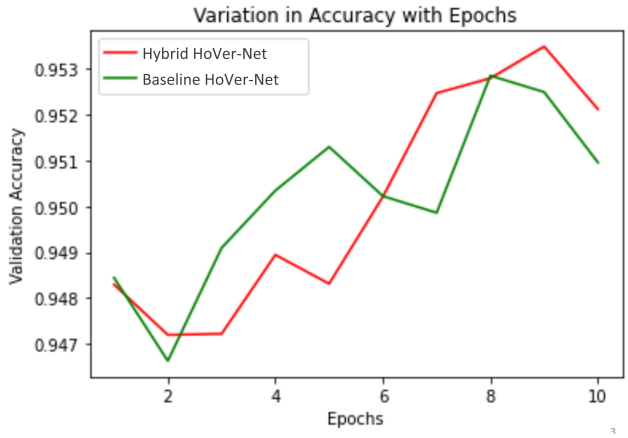

Fig. 5. Validation accuracy vs. the number of epochs for proposed and baseline model.

Table 1. Comparison between the proposed hybrid deep learning model and the baseline HoVer-Net model

Sr. No.	Validation Metric	Original HoVer-Net (B)	Modified HoVer-Net (C)	% Improvement = [(C-B)*100]/B
1	PQ	0.596	0.606	1.711
2	mPQ^{+}	0.437	0.444	1.596
3	R^2	0.714	0.775	8.536

vs. 0.595) and 1.59% (0.4435 vs. 0.4365) in PQ and mPQ^{+}, respectively, over the baseline HoVer-Net model. The nuclei cellular composition predicted using the proposed hybrid model and the baseline model is also compared using the multi-class coefficient of determination (R^2). The proposed model demonstrated an improvement of 8.5% in R^2 value over the baseline model (0.775355 vs. 0.714375). Table 2 also compares the proposed model and the baseline model during the training and validation phases. Rows 1, 2, and 3 in Table 2 show the comparison between the two models based on mean squared error, accuracy, and the dice score. From the results given in Table 1 and 2, the overall trend shows that the proposed model provides significantly better results for segmentation and classification compared to the baseline model. Note that both the proposed and baseline models are trained and evaluated for the same number of epochs. Although the overall training loss for both the models is comparable, the proposed model showed a significant improvement in the quantitative metrics such as validation accuracy and mean square error.

Fig. 5 shows the variation in validation accuracy vs. epochs from the proposed hybrid HoVer-Net and baseline HoVer-Net model for 10 epochs. From Fig. 5, it is observed that the accuracy of the proposed hybrid HoVer-Net model is increased after the 6th epoch as compared to the baseline HoVer-Net. Furthermore, a detailed comparative analysis was done among the performance of the proposed hybrid HoVer-Net model and other state-of-art literature as Naylor et al. (2018)

Table 2. Performance metrics during the inference phases for the proposed and baseline HoVer-Net model

Sr. No.	Metric	Original HoVer-Net (B)	Modified HoVer-Net (C)	% Improvement = [(C-B)*100]/B
1	Mean Squared Error Loss	0.041	0.039	-4.473
2	Accuracy	0.951	0.952	0.151
3	Dice Score	0.836	0.842	0.741

[25], Saha et al. (2018) [26] , Raza et al. (2018) [27], Dang et al. (2019) [28] and Graham et al. (2019) [9] using eight attributes and shown in Table 3.The majority of the available studies use the ResNet50-based model in their algorithms for image segmentation and classification. The proposed study uses a large number of images from the Lizard database provided by the CoNIC2022 challenge. Note that the proposed study extends the baseline HoVer-Net model by fusing the deep features with handcrafted features extracted using LBP and HoG which can combine both the sets of diverse features for colon nuclei segmentation, classification, and counting the number of cells in histology images. Moreover, Fig. 6 shows a few samples of source images out of the complete dataset and their corresponding predicted images from the proposed hybrid HoVer-Net model. From Fig. 6, it has been observed that the predicted images are compared with those with the ground truth images.

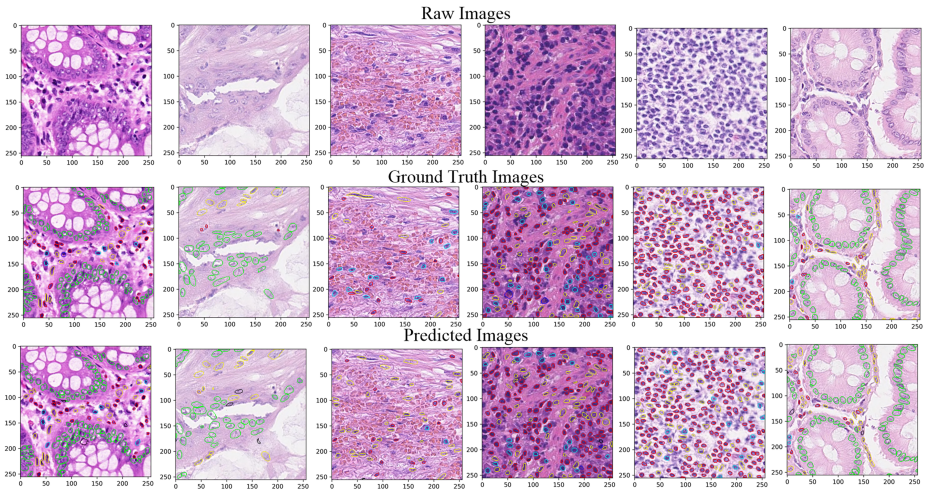

Fig. 6. The above figure shows six random image samples, taken from the dataset of H&E Stained Slides, as provided in the CoNIC Dataset. For each of the six images, the image in the first row is the raw image, which is to be segmented. The image in the second row is the ground truth showing the segments. The third row shows the predicted output for the respective images.

Table 3. Comparing the proposed with the state-of-the-art models

Sr. No.	Studies (Year)	Methods	Dataset	# Images	Handcrafted Features	Evaluation
1	Saha et al. (2018)	Her2Net	HER2 Image Database	158	No	Precision=96.64% , Recall=96.79%, F1-score=96.71%, Accuracy=98.33%
2	Naylor et al. (2018)	Regression task of Distance Map	Curie Institute and IIT Guwahati	80	No	F1 Score=0.789, AJI score=0.559, $Dice$=0.775, PQ = 0.432
3	Raza et al. (2018)	Micro-Net	Multiplexed Fluorescence Imaging Data, CPM and GLaS	229	No	$Dice$=0.792, AJI=0.615, PQ=0.542
4	Dang et al. (2019)	Modified Res-Net 50	NA	32	No	Dice Score average=0.777-0.783
5	Graham et al. (2019)	HoVer-Net	CoN-SeP	41	No	$Dice$=0.853, PQ=0.547
6	Proposed	Hybrid HoVer-Net	Lizard	4981	Yes	PQ=0.606, mPQ^+= 0.444, R^2=0.775

AJI: Aggregated Jaccard Index , PQ: Panoptic Quality, mPQ^+: multi-calss Panoptic Quality, NPV: Negative Predicted Value
All of the above-given models are used for Segmentation and Classification, but only the HoVer-Net and Hybrid HoVer-Net models perform cellular composition.

5 Conclusion

This paper presents a hybrid deep learning model by combining deep-learned and handcrafted features obtained from the feature descriptors such as local binary patterns and the histogram of oriented gradients. The proposed hybrid model has demonstrated a significant improvement in multi-class panoptic quality and multi-class panoptic quality metrics, which are the key metrics used for segmentation and classification tasks. The proposed study also shows the importance of texture-based feature descriptors in addition to the deep-learned features for colon nuclei segmentation, classification, and cell counting in H&E stained histology images. Though the proposed hybrid HoVer-Net model shows a significantly better performance compared to the baseline model, this still suffers from the noise sensitivity and higher computational time as LBP and HOG are considered as handcrafted feature extractors in the proposed model. Therefore, further studies will be done by integrating the other features and aligning with the histology images to provide more positive results.

References

1. T. A. A. Tosta, P. R. de Faria, L. A. Neves, and M. Z. do Nascimento, "Computational normalization of h&e-stained histological images: Progress, challenges and future potential," *Artificial Intelligence in Medicine*, vol. 95, pp. 118–132, 2019.
2. G. Campanella, M. G. Hanna, L. Geneslaw, A. Miraflor, V. Werneck Krauss Silva, K. J. Busam, E. Brogi, V. E. Reuter, D. S. Klimstra, and T. J. Fuchs, "Clinical-grade computational pathology using weakly supervised deep learning on whole slide images," *Nature Medicine*, vol. 25, no. 8, pp. 1301–1309, 2019.
3. L. Duran-Lopez, J. P. Dominguez-Morales, A. F. Conde-Martin, S. Vicente-Diaz, and A. Linares-Barranco, "Prometeo: A cnn-based computer-aided diagnosis system for wsi prostate cancer detection," *IEEE Access*, vol. 8, pp. 128 613–128 628, 2020.
4. S. Graham, M. Jahanifar, Q. D. Vu, G. Hadjigeorghiou, T. Leech, D. Snead, S. E. A. Raza, F. Minhas, and N. Rajpoot, "Conic: Colon nuclei identification and counting challenge 2022," *ArXiv Preprint arXiv:2111.14485*, 2021.
5. W. Liu, H. Wang, J. Du, and C. Jing, "Raman microspectroscopy of nucleus and cytoplasm for human colon cancer diagnosis," *Biosensors and Bioelectronics*, vol. 97, pp. 70–74, 2017.

6. A. Hamad, F. Bunyak, and I. Ersoy, "Nucleus classification in colon cancer h&e images using deep learning," *Microscopy and Microanalysis*, vol. 23, no. S1, pp. 1376–1377, 2017.
7. K. Sirinukunwattana, S. E. A. Raza, Y.-W. Tsang, D. R. Snead, I. A. Cree, and N. M. Rajpoot, "Locality sensitive deep learning for detection and classification of nuclei in routine colon cancer histology images," *IEEE Transactions on Medical Imaging*, vol. 35, no. 5, pp. 1196–1206, 2016.
8. H. Höfener, A. Homeyer, N. Weiss, J. Molin, C. F. Lundström, and H. K. Hahn, "Deep learning nuclei detection: A simple approach can deliver state-of-the-art results," *Computerized Medical Imaging and Graphics*, vol. 70, pp. 43–52, 2018.
9. S. Graham, Q. D. Vu, S. E. A. Raza, A. Azam, Y. W. Tsang, J. T. Kwak, and N. Rajpoot, "Hover-net: Simultaneous segmentation and classification of nuclei in multi-tissue histology images," *Medical Image Analysis*, vol. 58, p. 101563, 2019.
10. H. Khan, P. M. Shah, M. A. Shah, S. ul Islam, and J. J. Rodrigues, "Cascading handcrafted features and convolutional neural network for iot-enabled brain tumor segmentation," *Computer Communications*, vol. 153, pp. 196–207, 2020.
11. S. Graham, M. Jahanifar, A. Azam, M. Nimir, Y.-W. Tsang, K. Dodd, E. Hero, H. Sahota, A. Tank, K. Benes *et al.*, "Lizard: A large-scale dataset for colonic nuclear instance segmentation and classification," in *Proceedings of the IEEE/CVF International Conference on Computer Vision*, 2021, pp. 684–693.
12. E. S. Gedraite and M. Hadad, "Investigation on the effect of a gaussian blur in image filtering and segmentation," in *Proceedings ELMAR-2011.* IEEE, 2011, pp. 393–396.
13. S.-H. Lee and S. Kwon, "Median blur filter speed optimization for binary image," *Welcome Remarks*, p. 70, 2018.
14. D. T. Nguyen, T. D. Pham, N. R. Baek, and K. R. Park, "Combining deep and handcrafted image features for presentation attack detection in face recognition systems using visible-light camera sensors," *Sensors*, vol. 18, no. 3, p. 699, 2018.
15. N. Dalal and B. Triggs, "Histograms of oriented gradients for human detection," in *2005 IEEE Computer Society Conference on Computer Vision and Pattern Recognition (CVPR'05)*, vol. 1, 2005, pp. 886–893.
16. A. Aziz, A. Sohail, L. Fahad, M. Burhan, N. Wahab, and A. Khan, "Channel boosted convolutional neural network for classification of mitotic nuclei using histopathological images," in *2020 17th International Bhurban Conference on Applied Sciences and Technology (IBCAST).* IEEE, 2020, pp. 277–284.
17. L. Song, X. Liu, L. Ma, C. Zhou, X. Zhao, and Y. Zhao, "Using hog-lbp features and mmp learning to recognize imaging signs of lung lesions," in *2012 25th IEEE International Symposium on Computer-Based Medical Systems (CBMS).* IEEE, 2012, pp. 1–4.
18. T. Ojala, M. Pietikainen, and T. Maenpaa, "Multiresolution gray-scale and rotation invariant texture classification with local binary patterns," *IEEE Transactions on Pattern Analysis and Machine Intelligence*, vol. 24, no. 7, pp. 971–987, 2002.
19. D. J. Marceau, P. J. Howarth, J.-M. M. Dubois, D. J. Gratton *et al.*, "Evaluation of the grey-level co-occurrence matrix method for land-cover classification using spot imagery." *IEEE Transactions on Geoscience and Remote Sensing*, vol. 28, no. 4, pp. 513–519, 1990.
20. L. M. Bruce, C. H. Koger, and J. Li, "Dimensionality reduction of hyperspectral data using discrete wavelet transform feature extraction," *IEEE Transactions on geoscience and remote sensing*, vol. 40, no. 10, pp. 2331–2338, 2002.

21. M. Calonder, V. Lepetit, C. Strecha, and P. Fua, "Brief: Binary robust independent elementary features," in *European conference on computer vision*. Springer, 2010, pp. 778–792.
22. E. Rublee, V. Rabaud, K. Konolige, and G. Bradski, "Orb: An efficient alternative to sift or surf," in *2011 International conference on computer vision*. Ieee, 2011, pp. 2564–2571.
23. A. Kirillov, K. He, R. Girshick, C. Rother, and P. Dollár, "Panoptic segmentation," in *Proceedings of the IEEE/CVF Conference on Computer Vision and Pattern Recognition*, 2019, pp. 9404–9413.
24. S. Piramanayagam, E. Saber, W. Schwartzkopf, and F. W. Koehler, "Supervised classification of multisensor remotely sensed images using a deep learning framework," *Remote Sensing*, vol. 10, no. 9, p. 1429, 2018.
25. P. Naylor, M. Laé, F. Reyal, and T. Walter, "Segmentation of nuclei in histopathology images by deep regression of the distance map," *IEEE Transactions on Medical Imaging*, vol. 38, no. 2, pp. 448–459, 2018.
26. M. Saha and C. Chakraborty, "Her2net: A deep framework for semantic segmentation and classification of cell membranes and nuclei in breast cancer evaluation," *IEEE Transactions on Image Processing*, vol. 27, no. 5, pp. 2189–2200, 2018.
27. S. E. A. Raza, L. Cheung, M. Shaban, S. Graham, D. Epstein, S. Pelengaris, M. Khan, and N. M. Rajpoot, "Micro-net: A unified model for segmentation of various objects in microscopy images," *Medical Image Analysis*, vol. 52, pp. 160–173, 2019.
28. Q. D. Vu, S. Graham, T. Kurc, M. N. N. To, M. Shaban, T. Qaiser, N. A. Koohbanani, S. A. Khurram, J. Kalpathy-Cramer, T. Zhao *et al.*, "Methods for segmentation and classification of digital microscopy tissue images," *Frontiers in Bioengineering and Biotechnology*, p. 53, 2019.